NANO LETTERS

Letter

pubs.acs.org/NanoLett

Template-Induced Structure Transition in Sub-10 nm Self-Assembling Nanoparticles

Mohamed Asbahi,[†] Shafigh Mehraeen,[‡,§] Kevin T. P. Lim,[†] Fuke Wang,[†] Jianshu Cao,[‡] Mei Chee Tan,[§] and Joel K. W. Yang*[,†,§]

[†]Institute of Materials Research and Engineering, Agency for Science, Technology and Research (A*STAR), Singapore 117602

[‡]Department of Chemistry, Massachusetts Imstitute of Technology, Cambridge, Massachusetts 02139, United States

[§]Pillar of Engineering Product Development, Singapore University of Technology and Design, Singapore 138682

Supporting Information

ABSTRACT: We report on the directed self-assembly of sub-10 nm gold nanoparticles confined within a template comprising channels of gradually varying widths. When the colloidal lattice parameter is mismatched with the channel width, the nanoparticles rearrange and break their natural close-packed ordering, transiting through a range of structural configurations according to the constraints imposed by the channel. While much work has been done in assembling ordered configurations, studies of the transition regime between ordered states have been limited to microparticles under applied compression. Here, with coordinated experiments and Monte Carlo simulations we show that particles transit through a more diverse set of self-assembled configurations than observed for compressed systems. The new insight from this work could lead to the control and design of complex self-assembled patterns other than periodic arrays of ordered particles.

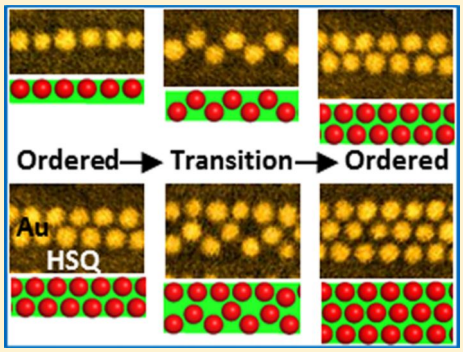

KEYWORDS: *Directed self-assembly, template-assisted self-assembly, structure transition, gold nanoparticles, sub-10 nm patterning, electron-beam lithography*

The patterning of sub-10 nm structures at high densities over large areas is currently limited by the resolution and throughput capabilities of existing top-down lithographic tools. To address these limitations, directed self-assembly of colloidal nanoparticles (DSA-n) within a template is emerging as a potential bottom-up technique to achieve ordering of close-packed structures within a two-dimensional (2D) monolayer.[1−3] Such systems are of great interest for many technologies such as plasmonics,[4] biosensing,[5] and magnetic bit patterned media[6] due to their ability to create gaps and pattern densities beyond the limits of lithography. Though they are immensely useful for creating periodic structures,[2] self-assembling nanoparticles are unfortunately still limited in the range of patterns that they can create. As a step toward achieving design guidelines for creating complex ensembles of nanoparticles, we explore the various configurations that arise as sub-10 nm gold nanoparticles are constrained to assemble within narrow channels of varying width.

In DSA-n using channels, confined particles spontaneously pack to form hexagonal arrays with integer multiples of rows that fit in commensuration with the width of the channels.[1,2] We have previously shown in the assembly of two or more rows that the array of particles can strain by up to 35% to maintain hexagonal packing as the width of the channel is varied.[2] However, when this variation becomes comparable to the colloidal diameter, finite-size effects such as the dislocation of the particles from their desired positions and reorientation of the lattice would occur. These effects can result in dramatic and often unpredictable changes in the physical properties of the system.[7,8] To understand these effects in macroscopic colloids, Pieranski[9,10] initiated a study of compression-induced structure transitions followed by extensive theoretical and experimental studies by others in both 2D[9−12] and 3D[13−15] colloidal systems.

To date, there have been no reports on the structure transition in DSA-n for sizes that are relevant for the technologies described above. Most of the reported studies on 3D structure transitions use particles with diameters ranging from several hundreds of nanometers to several micrometers.[11,14] These large particles allow for real-time particle tracking, for example, with optical microscopy of particles compressed between parallel glass plates[9] or wedged geometries.[14] Because of the external compression experienced by the particles, a unique structure transition sequence was reported as the compression was increased: $(n + 1)\Delta \rightarrow (n)\square \rightarrow (n)\Delta$, where n is the number of particle layers, and $\square$ and Δ correspond to square and hexagonal symmetry, respectively.[14,16]

Received: February 7, 2014
Revised: March 31, 2014
Published: April 4, 2014

   dx.doi.org/10.1021/nl5004976 | *Nano Lett.* 2014, 14, 2642−2646

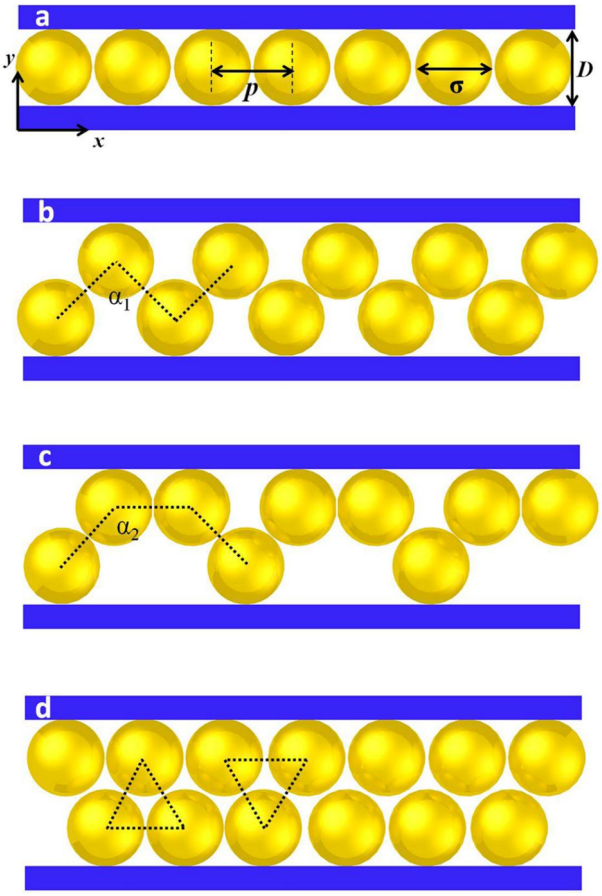

Figure 1. Schematic illustration of colloids of diameter σ and pitch p self-assembled within a channel with variable spacing D. (a,d) The packing of the particles when D is commensurate with the lattice parameter of the particles. (b,c) Two possible scenarios of transitional structures with different packing fractions when D does not match with the lattice parameter of the particles.

It is unclear if particles that self-assemble into 2D arrays within a template in the absence of compression would sequentially transit through the same configurations as demonstrated for compressed particles. For instance, Figure 1 depicts schematically the transition from 1 row (a) to 2 rows (d) of particles transiting through other possible configurations (e.g., b,c) with different packing fractions of $\Phi = 0.65$ and $\Phi = 0.57$ for the same channel width D, assuming an angle of $\alpha_1 = 90°$ for (b) and $\alpha_2 = 135°$ for (c). Packing fraction is defined as the area occupied by the particles divided by the occupied cell area. For compressed particles, it is observed that particles will rearrange to maximize packing fraction.[9] Thus, only the configuration with the larger packing fraction (b) would be possible. In this report, we show instead that packing-fraction maximization does not apply to DSA-n within a confining channel without external compression.

To observe the particles in a continuous transition, we patterned an array of channels that taper inward with a gradually decreasing width, as shown in Figure 2A. The channel widths were designed to fit only 1 to 3 rows of particles. The depth of the channels was ~15 nm, sufficient to accommodate a monolayer of particles. The colloids were spherical gold nanoparticles (AuNPs) with 8 nm core diameters that were synthesized by solution chemistry methods.[17] AuNPs were stabilized by a ~2 nm oleylamine shell and suspended in hexane (the total AuNPs diameter was 12 nm including the ligand shell). Templates were fabricated on silicon substrates by exposing lines in a negative-tone hydrogen silsesquioxane (HSQ) resist using a 100 kV electron beam lithography (EBL) system.[2] The resist was developed for 1 min with an aqueous solution of 1% NaOH and 4% NaCl, followed by rinsing under running deionized water for 1 min.[18] Templates were cleaned in a UV ozone cleaner for 5 min prior to nanoparticle deposition. The particles were then deposited onto the samples by drop-casting. During solvent evaporation, the particles were concentrated at the surface of the sample and attracted into the template by the capillary forces. Finally, the samples were imaged by a high-resolution field-emission scanning electron microscope (SEM). The images were analyzed in Matlab and ImageJ.[19]

Figure 2B shows a SEM image of the AuNPs self-assembled between HSQ lines of ~10 nm width under the effect of the template topography. At this level of magnification, we can observe five distinct circular zones (I–V) indicated by the dashed white lines. The influence of the template in directing the particles is clear, as there is a pronounced variation in particle coverage along the radial direction (in the direction of increasing channel width from I to V), but relatively uniform particle coverage along the circumferential direction (where the channel width is constant). This is evident from the observed radial symmetry of the self-assembled structure. The packing fraction oscillates between regions of high and low particle coverage as the channel width is varied. Here, the low particle coverage observed in zones (II and IV) is characteristic of the structure transition regime from n to $(n + 1)$ parallel rows of particles, whereas the dense packing in zones (I, III, and V) indicates that hexagonal close-packing is attained in those regions.

Next, we investigate the detailed assembly of particles within these zones to determine the various configurations that form. These configurations can be clearly observed in a high-resolution SEM image presented in Figure 2C where the zones (I, III, and V) show the commensurate packing of particles into 1, 2, and 3 rows, respectively. For close packing, commensuration is only achieved when the channel width $D(n) = \sigma(1 + (n - 1)\sqrt{3/2})$, $n \geq 1$, where the particle diameter σ is equal to the center-to-center spacing of the particles. As the spacing D increases, zone (II) shows the structure transiting gradually through a buckled structure, from one straight row to two parallel rows with triangular packing. Similarly, zone (IV) shows particles transiting through more complex configurations from two to three rows.

To understand the impact of particle–particle and particle–template interactions in our system, we performed Monte Carlo simulations of initially randomly distributed particles. The number of particles was varied from 280 to 320 in each simulation. We considered a simulation trapezoid equal to one of the lithographically defined channels with a total length of 2 μm. We ran each Monte Carlo simulation with total of 2×10^8 iteration steps. This number of iterations sufficiently equilibrated the total energy of the system. For simplicity, the energy of the system was considered to have only the Lennard-Jones pair potential[20,21] and the work done by the meniscus of the liquid on the particles. The capillary force was modeled as a downward force toward the bottom of the channel (more details in Supporting Information). Figure 2D shows a snapshot of the Monte Carlo simulation within a single channel,

dx.doi.org/10.1021/nl5004976 | Nano Lett. 2014, 14, 2642–2646

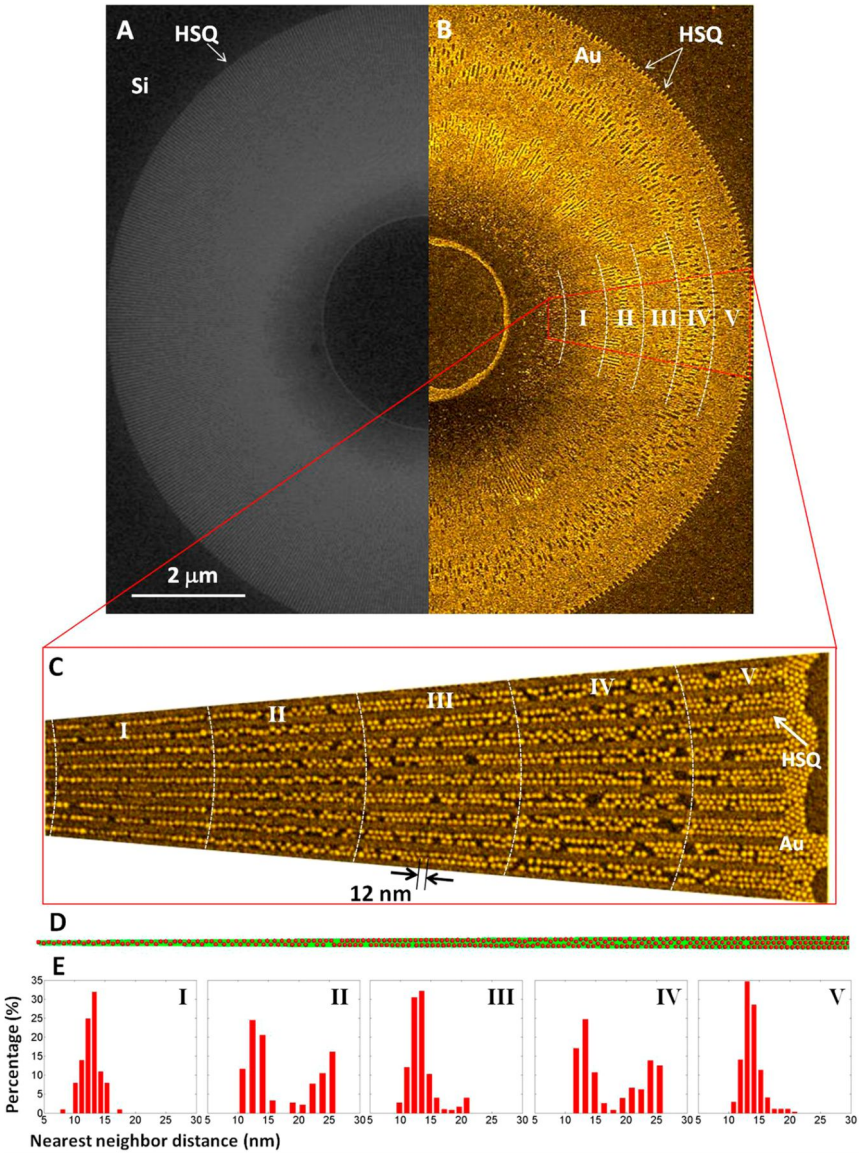

Figure 2. SEM micrographs showing (A) a HSQ grating template with variable spacing, (B) a monolayer of 12 nm diameter AuNPs (including the ligand shell) close packed within the template (A). The dashed lines are guides to the eye to highlight the different zones where the particles are packed in parallel rows to the grating zones (I, III, and V) as well as the transition zones (II and IV). The central zone is not considered, as the channels were below the resolution limit of electron beam lithography. (C) A high-resolution SEM micrograph of all the zones. (D) A snapshot of the Monte Carlo simulations reproducing the assembly of the particles as the channel width increases from left to right. The histograms (E) show the average percentage of nearest neighbors as a function of particle−particle distance in each corresponding zone obtained from the experimental data.

illustrating a similar trend to the particles in the SEM of Figure 2C. In both cases, the particles do not transit through a unique sequence of configurations. Further qualitative and quantitative comparison of theoretical prediction and experimental observation of these configurations will be discussed later in this section.

A clear distinction between the zones is obtained by measuring the center-to-center distances between the nearest neighbors for each individual zone and plotting their distributions as shown in the histograms of Figure 2E. The distributions for zones I, III, and V are similar and exhibit a single peak at ∼12 nm, indicating the presence of large blocks of ordered, close-packed particles. In contrast, the distributions for zones II and IV show a larger spread and a secondary peak appearing at ∼25 nm, accounting for the disordered and loose packing of the particles. However, the distribution at 12 nm is still larger than that at 25 nm, which demonstrates that the majority of the particles are still in contact with at least one other particle. From the SEM image in Figure 2C, one can see that most of the connected particles are also in contact with the walls of the channel, suggesting a capillary force between the HSQ walls and the particles. Consequently, when the packing is loose due to the mismatch between the particles lattice parameter and the channel width, the probability of particles sticking to the walls is much higher than the probability of forming rattlers, that is, isolated particles that do not touch any walls or another particle.

dx.doi.org/10.1021/nl5004976 | Nano Lett. 2014, 14, 2642−2646

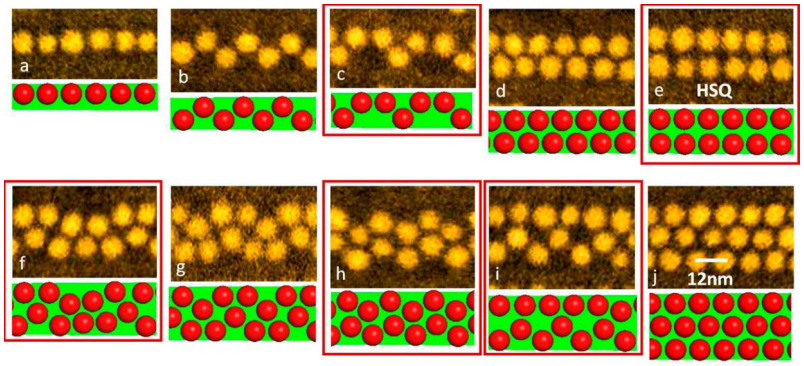

Figure 3. SEM micrographs (black and yellow) and zoom-in of Monte Carlo simulations (green and red) showing several possible configurations that the particles may transit through (b,c,e–i) to attain a more stable packing configuration (a,d,j). Additional configurations not typically observed in transitions of compressed systems are indicated (red boxes).

Importantly, within the order–disorder transition regime we observed that the particles do not transit through a unique sequence of configurations, unlike the case of a compressed system.

Nonetheless, dominant recurring configurations of particles can be identified to form within the channels as shown in Figure 3. The additional configurations that are not observed in the case of compressed systems are indicated for clarity. For the transition from one to two rows of particles, the transition configurations are equally likely because every particle experiences the same magnitude of capillary force to the HSQ walls. However, for the transition from two to three rows, the configurations with more particles sticking to the HSQ walls (e.g., square configuration, Figure 3e) are more probable than those with fewer particles touching the walls (e.g., one straight row and a buckled row, Figure 3i). Snapshots of the corresponding configurations were also observed in the Monte Carlo simulations as shown in Figure 3 beneath the SEM images. Given the simplicity of the model (using reasonable values from literature with no fitting parameters), the agreement between simulation and experiment is remarkable.

To test the assumption that particles will tend to rearrange to maximize their packing,[9] we measured the packing fraction of the particles as a function of the normalized channel width D/p, where p is the equilibrium pitch of the particles. We plotted the packing fraction against the normalized channel width as shown in Figure 4. Excellent agreement can be seen between the simulation results (red dots, averaged over 100 simulations) with experimental data (black dots). For comparison, we included the packing fraction from the model theory (blue curve) modified from Pieranski's model for a compressed system (details in Supporting Information).[9] The peaks at D/p = 1, 1.9, and 2.7 correspond to 1, 2, and 3 rows of close-packed particles, respectively.

The modified Pieranski model presents an upper limit to the achievable packing fraction in the transition configurations. As the model only considers structure transitions corresponding to Figures 3b,g, it does not account for those with lower packing fractions that appear as the scatter of data points below the blue curve. This scatter is indicative of the frequent occurrence of intermediate configurations reported in Figure 3 (c,e,f,h,i). A sampling of data points with their corresponding SEM images are indicated.

To account for the new configurations with lower packing fractions, we derived an analytical expression for the packing

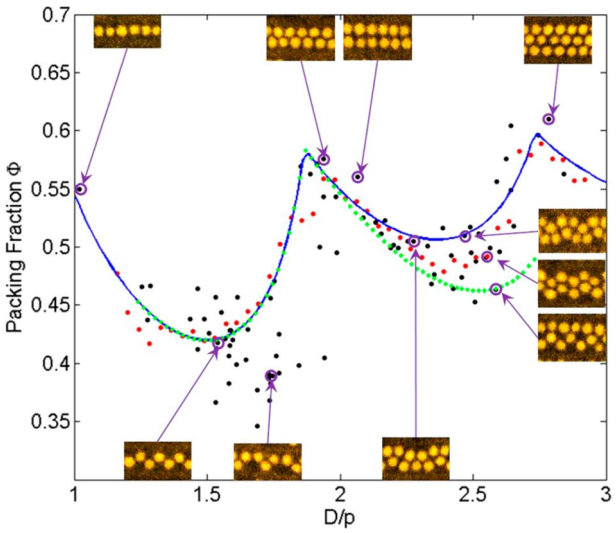

Figure 4. Packing fraction ϕ as a function of the normalized channel width between the gratings D/p, from experiment (black dots) and Monte Carlo simulation (red dots). The curves represent the modified Pieranski model (blue curve) and our analytical model (green curve). See Supporting Information for details of the models. The inset SEMs represent selected configurations to highlight the wealth of the structure transition represented by the scatter of the data.

fraction (see Supporting Information) shown by the green curve in Figure 4. In contrast to the Pieranski model (blue curve), the green curve does not consider the maximization of the packing fraction from 2 to 3 rows. This curve presents the packing fraction accounting the transition from 1 to 3 lines in three main stages. The first stage reproduces the Pieranski model for the transition from one straight line (Figure 3a) to two lines of particles in a hexagonal pattern (Figure 3d) going through the zigzag configuration (Figure 3b). However, the deviation from the Pieranski model begins in the second stage as we calculate the transition from the hexagonal (Figure 3d) to a square pattern (Figure 3e), which is not considered in the Pieranski model. In the third stage, our model accounts for a transition from two lines in the square pattern (Figure 3e) into a configuration of three lines of particles (Figure 3i) where one straight row assembles together with a buckled row.

The green curve shows that our model coincides with Pieranski's model for the transition from one row to two rows

dx.doi.org/10.1021/nl5004976 | Nano Lett. 2014, 14, 2642–2646

of particles as a result of the unique buckled structure transition considered by both models. However, in the transition from two to three rows, the green curve provides an approximate lower bound to the packing fraction data collected. We hypothesize that these other configurations that occur are due to the absence of external compression and might also be due to stretching that is sustained by the particle lattice. While these additional configurations might not be formed when rows of particles are compressed, it is easier to conceive how they might form if one stretches them sideways while maintaining compression along the channel, i.e. in transitioning from n = 1 to 3 instead of 3 to 1. Therefore, the behavior of sub-10 nm nanoparticles directed to assemble in mismatched channels appear to behave in a way different from particles under compression and possibly like particles under tensile stress. Ultimately, the assumption of packing-fraction maximization is not valid in the directed self-assembly of nanoparticles.

In conclusion, we have investigated both experimentally and via simulations the structure transition of a sub-10 nm 2D colloidal system induced by a channel template with varying width. We found that when nanoparticles were assembled in the predefined space and subjected only to the template potential, the resulting structures were unlike those predicted for compressed hard-sphere systems. Multiple alternative configurations were identified as forming combinations of zigzag and straight connections of particles. While this work focused only on gold nanoparticles with core sizes of sub-10 nm diameters and a soft ligand shell, similar behavior is expected also for particles of different materials of comparable sizes. The results point toward the possibility of using strategic template designs to engineer more complex patterns in nanoparticle assembly by introducing template structures that make one structure more energetically favorable than another.

■ ASSOCIATED CONTENT

Supporting Information

Theoretical models, Monte Carlo simulation, and template design. This material is available free of charge via the Internet at http://pubs.acs.org.

■ AUTHOR INFORMATION

Corresponding Author

*E-mail: joel_yang@sutd.edu.sg.

Notes

The authors declare no competing financial interest.

■ ACKNOWLEDGMENTS

This work was supported by the Agency for Science, Technology, and Research (A*STAR) in Singapore. The work made use of the SERC nano Fabrication, Processing, and Characterization (SnFPC) facilities in the Institute of Materials Research and Engineering (IMRE). S. Mehraeen, J. Cao, and M. C. Tan gratefully acknowledge the support from the SUTD-MIT Postdoctoral Fellows Programme. J.K.W.Y thanks the support from A*STAR SERC Grant 092 156 0119 and SUTD Startup Research Grant SRG EPD 2013 069.

■ REFERENCES

(1) Xia, Y.; Yin, Y.; Lu, Y.; McLellan, J. *Adv. Funct. Mater.* **2003**, *13*, 907−918.
(2) Asbahi, M.; Lim, K. T. P.; Wang, F.; Duan, H.; Thiyagarajah, N.; Ng, V.; Yang, J. K. W. *Langmuir* **2012**, *28*, 16782−16787.
(3) Ye, Y. H.; Badilescu, S.; Truong, V. V.; Rochon, P.; Natansohn, A. *Appl. Phys. Lett.* **2001**, *79*, 872−874.
(4) Fan, J. A.; Bao, K.; Sun, L.; Bao, J. M.; Manoharan, V. N.; Nordlander, P.; Capasso, F. *Nano Lett.* **2012**, *12*, 5318−5324.
(5) Wink, T.; vanZuilen, S. J.; Bult, A.; vanBennekom, W. P. *Analyst* **1997**, *122*, R43−R50.
(6) Yang, J. K. W.; Chen, Y. J.; Huang, T. L.; Duan, H. G.; Thiyagarajah, N.; Hui, H. K.; Leong, S. H.; Ng, V. *Nanotechnology* **2011**, *22*, 5301−5306.
(7) Scheeler, S. P.; Mühlig, S.; Rockstuhl, C.; Hasan, S. B.; Ullrich, S.; Neubrech, F.; Kudera, S.; Pacholski, C. *J. Phys. Chem. C* **2013**, *117*, 18634−18641.
(8) Asbahi, M.; Moritz, J.; Dieny, B.; Gourgon, C.; Perret, C.; van de Veerdonk, R. J. M. *J. Phys. D Appl. Phys.* **2010**, *43*, 385003.
(9) Pieranski, P.; Finney, J. *Acta Crystallogr., Sect. A* **1979**, *35*, 194−196.
(10) Pieranski, P. *Phys. Rev. Lett.* **1980**, *45*, 569−572.
(11) Ramiro-Manzano, F.; Bonet, E.; Rodriguez, I.; Meseguer, F. *Langmuir* **2010**, *26*, 4559−4562.
(12) Schmiedeberg, M.; Stark, H. *Phys. Rev. Lett.* **2008**, *101*, 218302.
(13) Neser, S.; Bechinger, C.; Leiderer, P.; Palberg, T. *Phys. Rev. Lett.* **1997**, *79*, 2348−2351.
(14) Oğuz, E. C.; Marechal, M.; Ramiro-Manzano, F.; Rodriguez, I.; Messina, R.; Meseguer, F. J.; Löwen, H. *Phys. Rev. Lett.* **2012**, *109*, 218301.
(15) Ramiro-Manzano, F.; Meseguer, F.; Bonet, E.; Rodriguez, I. *Phys. Rev. Lett.* **2006**, *97*, 028304.
(16) Pieranski, P.; Strzelecki, L.; Pansu, B. *Phys. Rev. Lett.* **1983**, *50*, 900−903.
(17) Lau, C. Y.; Duan, H.; Wang, F.; He, C. B.; Low, H. Y.; Yang, J. K. W. *Langmuir* **2011**, *27*, 3355−3360.
(18) Yang, J. K. W.; Berggren, K. K. *J. Vac. Sci. Technol., B* **2007**, *25*, 2025−2029.
(19) Rasband, W. S. *ImageJ*; U. S. National Institutes of Health: Bethesda, MD; 1997, http://imagej.nih.gov/ij/ (accessed August 13, 2012).
(20) Frenkel, D.; Smith, B. *Understanding molecular simulation: from algorithms to applications*; Academic Press: San Diego, 2002.
(21) Nagata, I. *Can. J. Chem.* **1966**, *44*, 2651.